JJEE

Volume 12 | Number 2 | June 2026 | Pages 324-344

Jordan Journal of Electrical Engineering

ISSN (print): 2409-9600, ISSN (online): 2409-9619

Homepage: jjee.ttu.edu.jo

Performance Enhancement of a Photovoltaic-Powered Train Traction System Using Intelligent MPPT Technique

Mohamed Sharawy[1], Ahmed Elsayed Helal[2*], Islam Mohamed Abdelqawee[3]

[1, 2, 3] Electrical Engineering Department, Faculty of Engineering at Shoubra, Benha University, Cairo, Egypt
E-mail: ahmed.helal@feng.bu.edu.eg

Received: Nov 28, 2025 *Revised: Jan 22, 2026* *Accepted: Feb 25, 2026* *Available online: Jun 15, 2026*

***Abstract*—** This paper proposes the ability to install Photovoltaic (PV) panels onto train rooftops to generate electric power. The system mainly consists of PV modules, a DC-DC converter with a maximum power point tracking (MPPT) method, and a three-phase inverter feeding a permanent magnet synchronous motor (PMSM) as traction motors, besides other components. This article has managed to overcome a common problem for this application, the partial shading condition (PSC) of PV systems. Particle swarm optimization (PSO) algorithm is used to overcome this problem. The accuracy of the suggested algorithm was confirmed utilizing MATLAB SIMULINK. A financial feasibility study of the practical application was also presented, yielding a payback period of 10.5 years and savings exceeding 837,000 Egyptian pounds over the system's lifetime. According to the simulation results, the PMSM functioned well across a range of speed scenarios. The P&O can effectively track MPP of PV modules in conditions of uniform irradiance. However, during PSC, MPPT is switched to the PSO technique, which performs better than the P&O approach in tracking global MPP while maintaining an efficient PMSM operation.

***Keywords*—** Electrified railways; Photovoltaic; Partial shading; Permanent magnet synchronous motor; MPPT.

1. INTRODUCTION

Nowadays, the transport field directly affects both the energy and environment fields, especially electrified railways [1]. A variety of factors, including increased transportation capacity, time savings, environmental conservation led to the development of electric railways [2-4]. This progress naturally leads to increased carbon dioxide emissions [5]. According to the annual report of the World Energy Outlook 2024, this field accounts for around 27% of overall energy consumption. The growth of this field causes the total amount of energy used in 2023 to rise by 1.7%. Furthermore, it produces around 21.2% of all CO_2 emissions brought on by fuel burning. As illustrated in Fig. 1, Industry and transport contribute most of the total emissions from final consumption, but transport sees the biggest drop in emissions intensity thanks to rising electrification [6].

From points of view of the environment, society, and economy, the conventional transportation system is unsustainable [7]. The limitations of traditional systems in handling the increased power needed have been demonstrated by the necessity to expand its capacity [7]. The cost of diesel gasoline is increasing every day. In addition, using conventional power plants to meet the high demand for electricity may increase hazardous emissions. As a result,

* Corresponding author
DOI: https://doi.org/ 10.5455/jjee.204-1764347623

new technologies have been created to increase railway systems' energy efficiency. Among these technologies is the use of renewable energy sources [8].

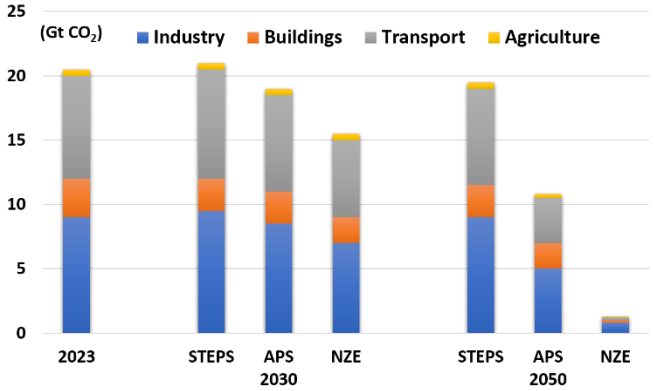

Fig. 1. CO_2 emissions by end-use sector and scenario, 2023, 2030 and 2050.

Electrified railway is a crucial component of the global transportation hub, which has been actively developed and supported by nations worldwide [9]. It is perhaps the safest, cleanest, and most efficient of all the transportation networks. Many additional benefits have contributed to the rise in popularity of electric train systems. such are increased power efficiency, a better power/weight ratio, traffic capacity, lower operating and maintenance expenses, and less noise. These features make it a crucial part of transportation networks in the future. So, Photovoltaic (PV) generation is suggested as an extension to supply power in railway systems [8].

There are several ways to integrate PV into a railway system. Railway stations can use their roofs and other structures for solar installations to power station operations and lessen their dependency on the grid. Also, PV panels can be installed along railroad tracks or on train roofs to produce electricity for auxiliary systems or traction power. [10]. The Byron Bay Railroad Company, for instance, converted a diesel locomotive into a solar-powered train with batteries in 2018 [11]. The train is powered solely by solar energy. The train is powered by 23 percent of the energy generated by solar panels on the roof of the train shed, which supply the onboard batteries, in addition to electricity generated by panels on the train's roof. A green energy supplier feeds the remaining 77% into the grid to power the neighborhood. Regenerative braking is another feature of the train that uses braking energy to replenish the batteries as it slows down [12].

Extracted power from PV significantly improves energy security, national income, public health, and environmental preservation. It has emerged as the most attracted and, in certain situations, the least expensive method of producing new power worldwide [13-14]. From Fig. 2, The biggest contributor to the expansion of the overall energy supply was renewables (38%) [15]. Due to PV's benefits in terms of its great flexibility and expandability, solar PV technologies and systems have grown rapidly over the past ten years on a global scale [7]. According to Fig. 3, Global yearly additions to renewable capacity increased by an expected 25% to around 700 GW in 2024. Moreover three-quarters of renewable capacity increases came from solar PV [15]. In 2024, solar PV installations increased by over 30% year over year to reach roughly 550 GW. As a result of this expansion, the estimated installed solar PV capacity globally reached 2.2 terawatts (TW) [8].

Research on high efficiency and life cycle cost has been increasingly important in driving systems such as railroads in recent years. Specifically, the traction motor determines the drive

system's performance and has the most impact on the output. As a result, a lot of research is being done on motor design, and Permanent Magnet Synchronous Motor (PMSM) is increasingly replacing induction motors [16]. PMSMs have become more popular in high-speed rail (HSR) applications in recent years [17]. They have good performance and robustness, low maintenance costs, high efficiency, a high power-to-weight ratio, and extremely good controllability over the whole speed serving range [18]. Such as, Alstom built AGV Italo, and Alstom and Bombardier built SNCF TVG and Eurostar. These are a few of the European HSR systems that employ PMSM as a traction motor [19]. To feed this load, The PV system consists of parallel and series arrangements of PV panels to meet the voltage and current requirements [20]. Often some panels are frequently exposed to shade from nearby buildings, trees, poles, birds, clouds [21]. This non-uniform irradiance condition is represented as a partial shading condition (PSC). PSC increases the non- linearity in the characteristic curves, causes multiple peaks in the characteristics of the PV array and lowers the efficiency of the system.

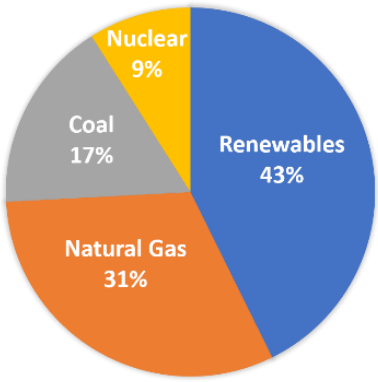

Fig. 2. Global demand growth, 2024.

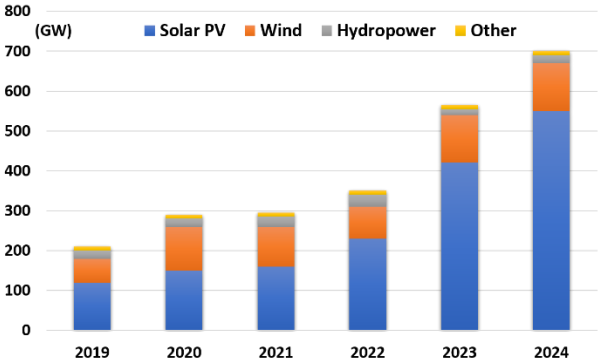

Fig. 3. Total renewable capacity additions, 2019-2024.

A bypass diode is linked across each module to offer an alternate path for excess current to reduce the hot spot effect. The PV characteristic exhibits extremely complicated behavior [22]. As illustrated in Fig. 4, there is only one absolute peak, known as global maximum power point (MPP), and several false peaks, known as local MPP. As a result, the conventional maximum power point tracking (MPPT) techniques are not suitable in PSC as they are not able to distinguish between global MPP and local MPP. Global MPPT strategies, which include optimization, intelligent control, and trial-and-error procedures, include multiple new innovative and easy MPPT concepts [23]. Particle swarm optimization (PSO) is the most common and reliable technique, and there are a number of papers that go into great

works on MPPT approaches [20, 22, 24-26]. The technology integrates PV panels on train roofs to generate power which assist the grid feed train loads. keeping up with Egypt's advancements in all fields, particularly in the energy and environmental fields. That accomplishing Egypt's Vision 2030's third strategic aim, "Integrated and Sustainable Environmental System"[27]. This system can be applied on Talgo 230 train in Cairo Light Rail Transit which is linking the city of Cairo to Egypt's New Administrative Capital and the 10th of Ramadan City. Fig. 5 shows that this location has a specific PV power output of 1890.6 kWh/kWp per year, which is good value to utilize a PV system [28]. Installing PV modules on train roofs has some challenges. These include low efficiency and exposure to partial and full shading due to various environmental and surrounding factors. So, PSC, full shading condition (FSC), and low efficiency are the challenges the system faces in this application and have a negative effect on system performance and reliability. The performance and reliability of the train in these conditions have not been examined by papers, nor have they offered solutions for them.

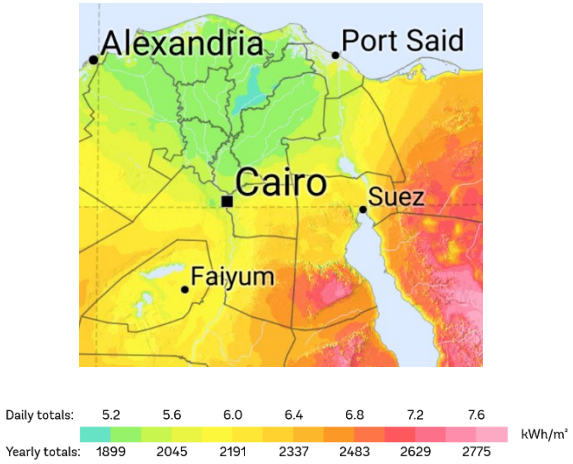

Average Hourly Profile – Direct Normal Irradiation [Wh/m²]												
Hour	Jan	Feb	Mar	Apr	May	Jun	Jul	Aug	Sep	Oct	Nov	Dec
0-6												
6-7				6	43	51	41	8				
7-8		3	56	165	281	310	279	203	181	66	15	
8-9	121	228	313	348	457	512	494	431	405	366	290	230
9-10	434	434	472	496	600	664	664	630	573	518	498	470
10-11	558	553	587	610	695	756	760	748	692	613	607	583
11-12	630	615	655	668	739	801	807	803	753	663	645	641
12-13	637	617	667	690	755	815	824	820	768	666	627	646
13-14	603	594	659	684	748	813	822	810	751	641	598	609
14-15	544	553	628	656	717	791	798	780	705	590	538	552
15-16	464	492	579	587	651	738	748	720	627	509	462	461
16-17	359	401	471	484	557	651	662	635	530	394	347	349
17-18	106	242	347	358	441	535	548	513	368	127	70	67
18-19		13	87	105	241	374	386	276	59			
19-20					3	57	60	4				
20-24												
Sum	4,456	4,746	5,521	5,858	6,928	7,868	7,892	7,382	6,411	5,153	4,697	4,610

Fig. 5. Solar atlas at new administrative capital, Cairo, Egypt.

Due to the importance of the topic, this paper introduces a complete model of the system and then makes a study of different MPPT techniques at different operating conditions. The novelty of this paper lies in:

- Provide a control strategy that uses the system voltage information to distinguish between the P&O method and the PSO approach depending on the nature of solar radiation.
- Evaluating the performance level of the dynamic system of the train traction motors under the operation of the MPPT techniques during partial shading on the surfaces of the trains during travel and monitoring the effect of this on the parameters of motor performance in terms of the effect on speed, speed distortion, alternating current, and power drawn when the mechanical load is constant.
- The MPPT methods used operate in a live manner. Since the trains are constantly moving, the PV modules on the train roofs are exposed to fast-varying and asymmetric solar radiation patterns around the clock. enabling the MPPT methods to extract the maximum possible electrical power from the PV system under all conditions.

- Submit a preliminary financial study of the proposed system and explain its practical feasibility.
- This study operated for the first time in an electrified train application.

This study gives acceptable results for the overall system performance and reliability by utilizing MATLAB SIMULINK.

2. SYSTEM DESCRIPTION

It is typical and widely accepted that trains are between 200 and 600 kW of power and 3 to 12 carriages [29]. Thus, the suggested train can be operated with 10 cars and an average motors power of 300 hp. By taking dimensions of The Talgo 230 roof, PV modules can be counted as they are related to their dimensions and that of the carriage roof. These dimensions are 40 meters long per carriage and 3 meters wide on average. The PV system is constructed using the SPR-X20-445-COM module, which has the rating shown in Table 1. Based on the information provided, that makes the ability to place around 35 modules on a single carriage roof as demonstrated in Fig. 6, providing a system with 15,575 W of electricity. There are two traction methods that can be used in an electric train are distributed traction (DT) and concentrated traction (CT), as seen in Fig. 7. When the DT and CT are compared, the DT uses less energy per passenger than the CT does. Additionally, the CT has a heavier train weight. The DT is superior to the CT for per unsprung mass for axle load. DT has recently attracted a lot of interest due to its benefits [30].

Table 1. SPR-X20-445-COM ratings at STC.

Parameter	Value	Unit
Nominal Power	445	W
Maximum Power Voltage (V_{MPP})	76.5	V
Maximum Power Current (I_{MPP})	5.82	A
Open Circuit Voltage (V_{OC})	90.0	V
Short Circuit Current (I_{SC})	6.24	A
Dimensions	(2067/1046)	mm

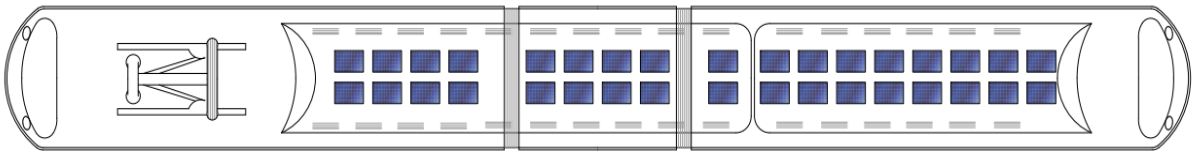

Fig. 6. PV system arrangement on train roof.

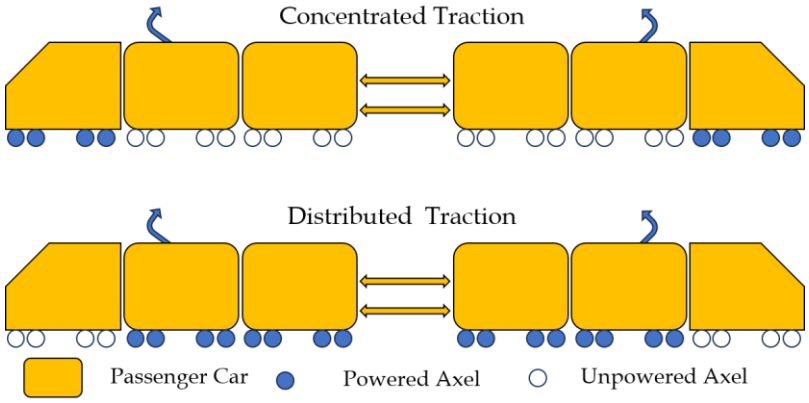

Fig. 7. Concentrated and distributed tractions.

As two motors are typically utilized in each car, there are around sixteen used motors in total. With the values listed in Table 2, each motor has about 17.7 horsepower. This proposed system is represented in Fig. 8 and can be represented in a block diagram as illustrated in Fig. 9. PV modules make up the system's secondary source. The suggested system focuses on a DC-DC converter that uses an MPPT approach to extract maximum power from a PV system under various irradiation situations. A PMSM is fed traction motors through a three-phase inverter equipped with Field-Oriented Control (FOC).

Table 2. PMSM parameters.

Parameter	Value	Unit
Power	17.7	hp
Speed	3000	RPM
Stator Resistance	0.0485	Ohm
Armature Inductance	0.000395	H
Pole Pairs	4	Poles
Inertia	0.0027	kg.m2
Damping	0.0004924	N.m.s

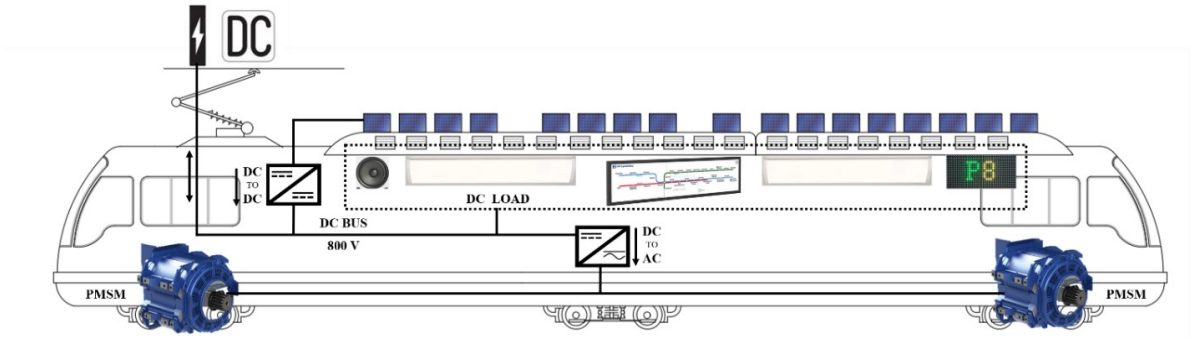

Fig. 8. System overview representation.

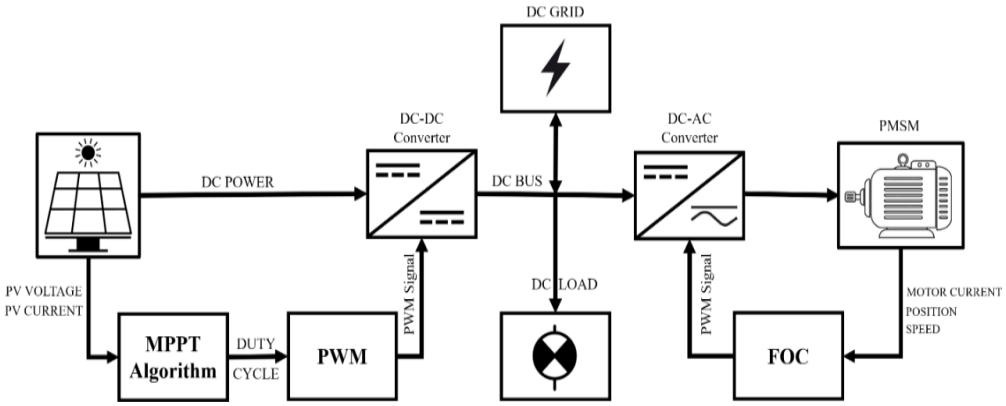

Fig. 9. System block diagram.

3. MODELLING OF THE SYSTEM

3.1. PV System

PV cells can be represented by equivalent circuit as illustrated in Fig. 10. I_{Ph} represents the cell photocurrent. I_o represents the cell saturation current. R_P and R_s are intrinsic shunts and series resistances of the cell respectively. PV module consists of a number of PV cells connected in parallel and series [31].

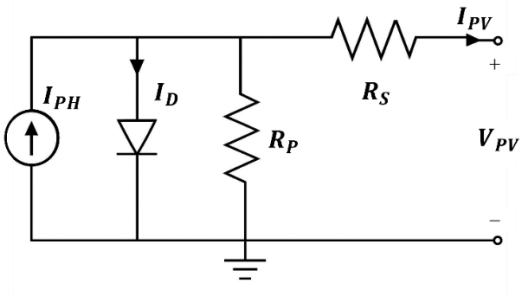

Fig. 10. PV cell equivalent circuit.

The PV module output current (I_{PV}):

$$I_{PV} = N_P * \left[I_{Ph} - I_o * \left[\exp\left(\frac{q*(V_{PV}+I_{PV}*R_S)}{N_s*k*A*T}\right) - 1\right] - \frac{(V_{PV}+I_{PV}*R_S)}{N_s*R_P}\right] \quad (1)$$

where V_{PV} is the output voltage, N_p and N_s are the number of PV cells connected in parallel and series for a given PV module, A is the ideality factor of the p–n junction, k is the Boltzmann's constant ($1.3806503 \times 10^{-23}$ J/K), T is the cell temperature in Kelvin, q is the charge of electron (1.6×10^{-19} C) [31].

PV photocurrent (I_{ph}):

$$I_{Ph} = [I_{SCC-STC} + k_i * (T - T_{STC})] * \frac{G}{G_{STC}} \quad (2)$$

where $I_{SCC-STC}$ refers to the short-circuit current (SCC) at standard test conditions (STC) in amperes, T_{STC} (25°C) is the cell temperature at STC, G (in watts per square meters, W/m^2) is the irradiation on the cell surface, G_{STC} ($1000W/m^2$) is the irradiation at STC and k_i is the SCC coefficient in in amperes per degree Celsius (A/℃) [31].

PV saturation current (I_o):

$$I_o = I_{rs} * \left[\frac{T}{T_{STC}}\right]^3 * \exp\left[\frac{q*E_g}{A*K}\left(\frac{1}{T_{STC}} - \frac{1}{T}\right)\right] \quad (3)$$

where E_g is the band gap for silicon = 1.1 eV [31].

PV reverse saturation current (I_{rs}):

$$I_{rs} = \frac{I_{SCC-STC}}{\left[\exp\left(\frac{q*V_{OC}}{N_s*k*A*T}\right)-1\right]} \quad (4)$$

where V_{OC} (in volt, V) is the open circuit voltage at STC. The characteristics of the PV module are indicated in Fig. 11 [31].

3.2. DC-DC Boost Converter

The boost converter in Fig. 12 is used to magnification the PV system output voltage to a desired value. Where V_o is the boost converter output voltage, V_s is the boost converter voltage The inductance, capacitance and switching frequency values are designed for continuous current and reduced ripple content in the boost converter [32].

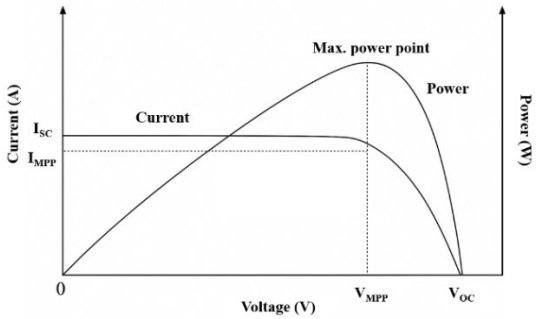

Fig. 11. I-V and P-V curves under normal condition.

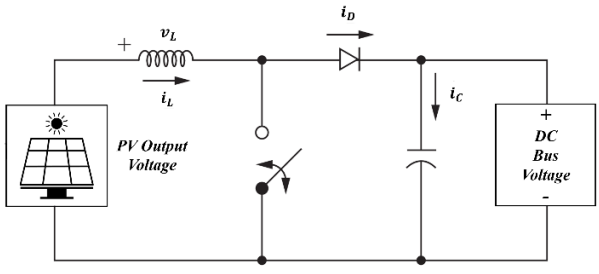

Fig. 12. The boost converter.

3.3. Permanent Magnet Synchronous Motor

PMSM uses a permanent magnet that behaves as a rotor [33]. PMSMs have a good performance specification [34]. It is possible to convert the dynamic model of synchronous machines into a rotating dq reference frame. taking into account a few assumptions [35]. The analogous circuit of the synchronous machine in the synchronous reference frame is displayed in Fig. 13. The corresponding equations for motion, torque, flux, and voltage are given [29].

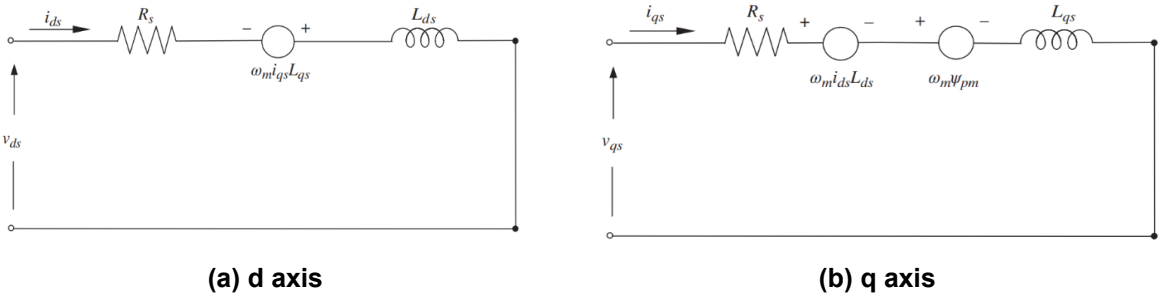

(a) d axis **(b) q axis**

Fig. 13. Equivalent Circuit for the d and q axis of a Synchronous Machine.

Voltage equation:

$$v_{ds} = R_s * i_{ds} + P\,\Psi_{ds} - \omega_m * \Psi_{qs} \quad (5)$$

$$v_{qs} = R_s * i_{qs} + P\,\Psi_{qs} - \omega_m * \Psi_{ds} \quad (6)$$

Flux equation:

$$\Psi_{ds} = L_{ds} * i_{ds} + \Psi_f \quad (7)$$

$$\Psi_{qs} = L_{qs} * i_{qs} \quad (8)$$

Torque equation:

$$T_e = \frac{3}{2} n_p * \left[\Psi_f * i_{qs} + (L_{ds} - L_{qs}) * i_{ds} * i_{qs}\right] \quad (9)$$

The formula above may be expressed as follows since L_{ds} and L_{qs} for the surface permanent magnet synchronous motor (SPMSM) have the same value:

$$T_e = \frac{3}{2} n_p * \Psi_f * i_{qs} \quad (10)$$

Motion equation:

$$T_e = J * P\left(\frac{\omega_m}{n_p}\right) + R_\Omega * \frac{\omega_m}{n_p} + T_L \quad (11)$$

The aforementioned equations have the following components: ψ_{ds} and ψ_{qs} are the d- and q-axis components of stator flux. L_{ds} and L_{qs} are the d- and q-axis equivalent inductances of stator windings. i_{ds} and i_{qs} are the d and q axis components of stator current. v_{ds} and v_{qs} are the d- and q-axis components of stator voltage. ψ_f is the flux of PMSM. R_s is the stator winding resistance. ω_m is the rotor speed. P is the differential operator. n_p is the number of pole pairs. T_e α i_q. T_L stands for load torque, and R_Ω is the damping coefficient; J is rotational inertia. The vector control approach of "i_{ds} = 0" is reflected in Eq. (10); that is, the torque is a function of solely the torque component of current (i_{qs}) and reaches it's maximum when i_{ds} = 0 [35].

4. CONTROL STRATEGIES

4.1. Maximum Power Point Tracking

Maximum power is generated by running PV modules at V_{MPP}. So, MPPT technique extracts this power by operating at this point. At uniform irradiance conditions the used technique is Perturb and Observe (P&O). Which is among the least complicated methods. The train length causes train cars to have varying irradiance levels, resulting in non-uniform

irradiance conditions. In this situation, A PSO technique is utilized. PSO has been regarded as one of the most widely employed techniques in the MPPT field in recent years [36]. Since PSO is conceptually in relation to search optimization, it can find the MPP for any type of P-V curve, based on the objective function of Eq. (12), regardless of environmental variations.

$$P_{pv} = V_{pv} * \ I_{pv} \tag{12}$$

The PSO method's broader formulation:

$$x_i^{k+1} = x_i^k + \ v_i^{k+1} \tag{13}$$

In which v_i stands for the velocity factor, which is determined by:

$$v_i^{k+1} = \omega * v_i^k + c_1 r_1 (P_{besti} - x_i^k) + c_2 r_2 (G_{besti} - x_i^k) \tag{14}$$

where ω=0.4 as the inertia weight, c_1 =1.2 and c_2 =2 as the acceleration constants, and P_{best} and G_{best} as the global and personal best positions, respectively. The method sends the computed duty cycles to the power converter after initializing a solution vector of voltage samples. In the initial iteration, these voltage samples (shown by x_i in Eq. (13)) behave as the starting particles. All of the particles thus move in the direction of their local best position, P_{best}. One of these particles is the best G_{best} in the globe. It offers the finest value for fitness. A new voltage location is obtained following the computation of the velocity, which acts as a displacement to the voltage. All particles go in the direction of the global optimal location through consecutive iteration. The particles approach the G_{best} position as they approach the MPP. The velocity term's P_{best} and G_{best} components correspondingly approach zero. Eventually, the voltage position stays almost constant, and a point of zero velocity is achieved. The PV system hits MPP in this instance.

4.2. Field-Oriented Control

FOC approach is utilized to adjust PMSM speed in order to make the train run at various speeds. Fig. 14 shows the structural diagram of the FOC system in PMSM [35]. FOC regulates the gate control signals of IGBTs to achieve the desired voltage magnitude and frequency at the inverter's output in the flowchart depicted in Fig. 15 [37].

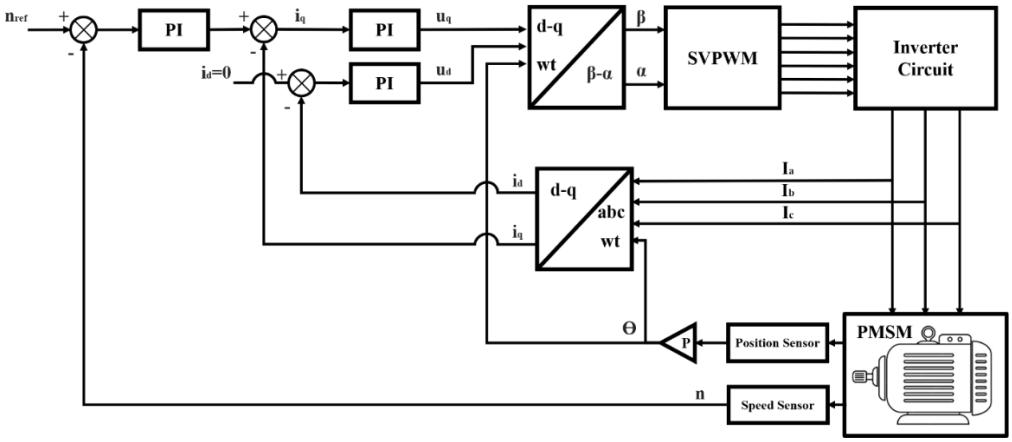

Fig. 14. PMSM FOC system block diagram.

5. SIMULATION RESULTS AND DISCUSSION

The system has been simulated using MATLAB/SIMULINK program. The system is tested under a variety of train operating settings. the various parameters such as PMSM functioning, PV output power, and DC grid power were observed how performed under these conditions. Fig. 16. Provide a control strategy that uses the system voltage information to

distinguish between the P&O method and the PSO approach depending on the nature of solar radiation. Further placing a cheap voltage sensor on a random panel to measure the voltage it generates. In order to determine if the solar radiation is uniform or whether the system is partially shaded, multiply this voltage by the number of panels linked in series, which is five. Then, compare the resulting voltage with the voltage of the complete system.

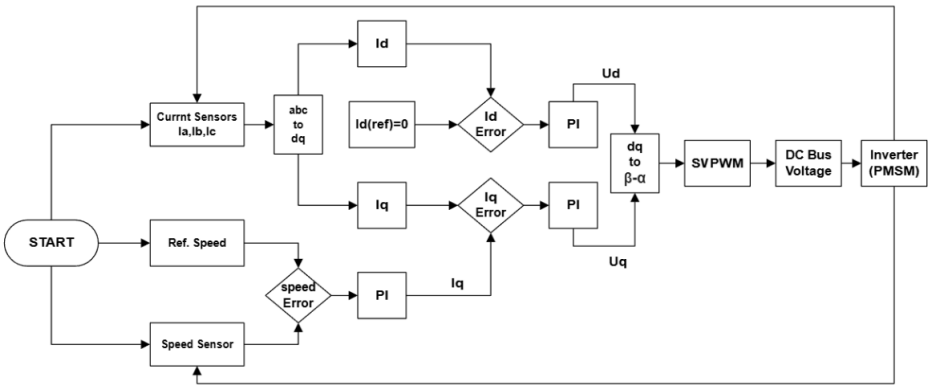

Fig. 15. PMSM FOC flowchart.

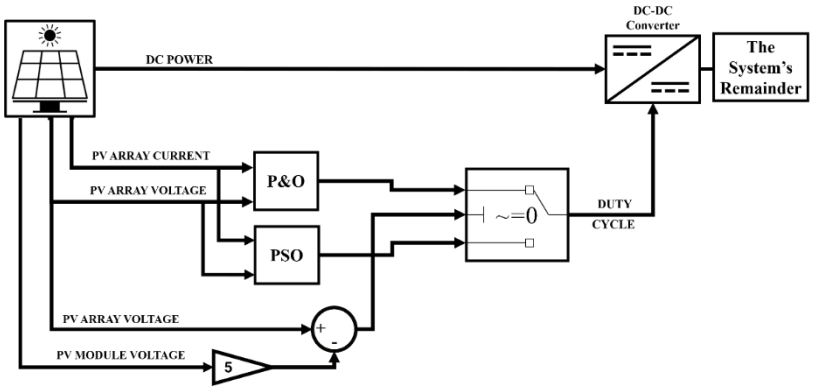

Fig. 16. Switching Control Strategy Between P&O Method and PSO Approach.

- Case study (1): The train moves under uniform irradiance conditions: In this case a random irradiance pattern is made which covers different uniform irradiance conditions with zero irradiance case as a simulation for train run through tunnel as indicated in Fig. 17 with a constant temperature of 25℃. At all conditions, DC bus voltage is constant at 800 V, and DC load, which covers different services inside the train, is assumed to be 6400 W (100 Ω). Despite irradiance has different values but still represent a uniform irradiance condition as these different values applied to whole PV modules in the system. So, P&O approach is used.

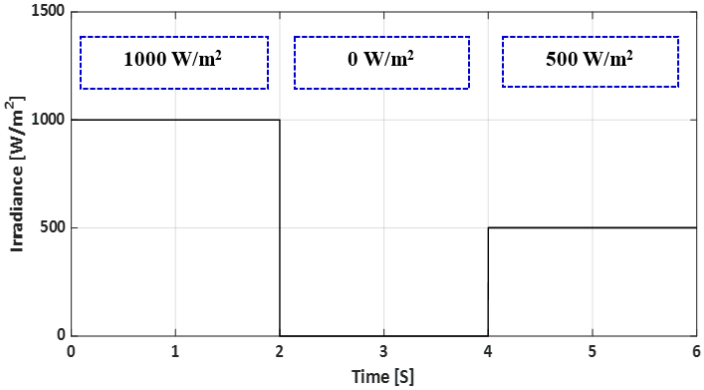

Fig. 17. Irradiance pattern.

Fig. 20 displays the reference speed and the motor speed simulation results. Two different events for speed change are described in Table 3. Fig. 21 shows the phase (A) motor current, which has a peak fundamental value of 56.2 A with Total Harmonic Distortion (THD) = 9.31% as shown in Fig. 18 in the first indicated event and a peak fundamental value of 56.17 A with THD = 7.92% as shown in Fig. 19 in the second indicated event.

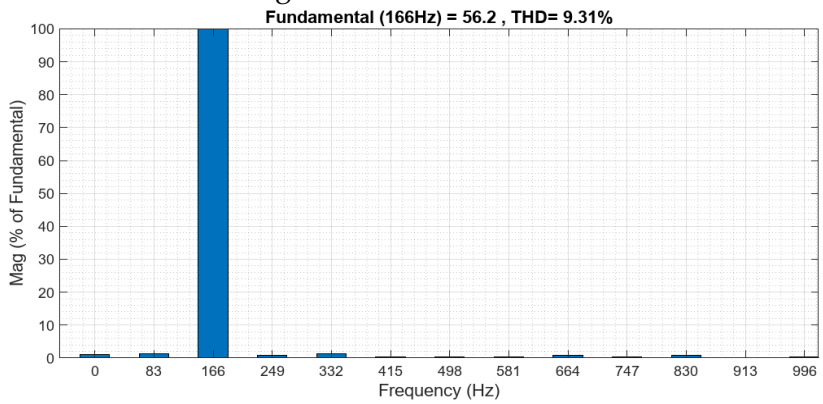

Fig. 18. THD of PMSM current at 2500 RPM.

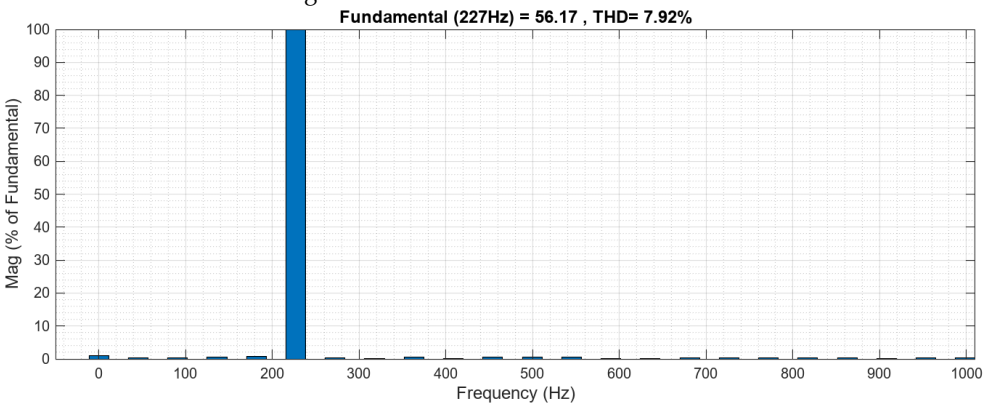

Fig. 19. THD of PMSM Current at 3400 RPM.

Table 3. Motor speed results analysis.

Steady state speed	3000	2700	RPM
Settling time	0.012	0.018	Sec
Peak transient speed	3118.5	2710	RPM
Min. transient speed	2992.5	2539	RPM
Max. Overshoot	+3.95	-5.96	%

Figs. (22-25) display generated power from the PV system, shared power by the DC grid and consumed power in loads. Power analysis at different operating events is summarized in Table 4.

Table 4. System power analysis.

Conditions [25°C]	Irradiance [W/m²]			1000			0			500		
	Motor speed [RPM]			3000			2700			2800		
Loads [Kw]	Minimum Instantaneous Value	Inverter Power	Maximum Instantaneous Value	13.2	13.4	16.1	8.5	12.3	12.5	12.4	14.6	13.2
		DC Load Power		6.4			6.4			6.4		
		Total System Avg. Power		19.6	19.8	22.5	14.9	18.7	18.9	18.8	19	19.6
Sources [Kw]		PV Power		14.78	15.1	15.3	0	6.9	7.5	7.3	14.7	15.1
		DC Grid Avg. Power		4.42	4.65	7.67	18.5	18.7	18.9	11.6	13.6	12.1

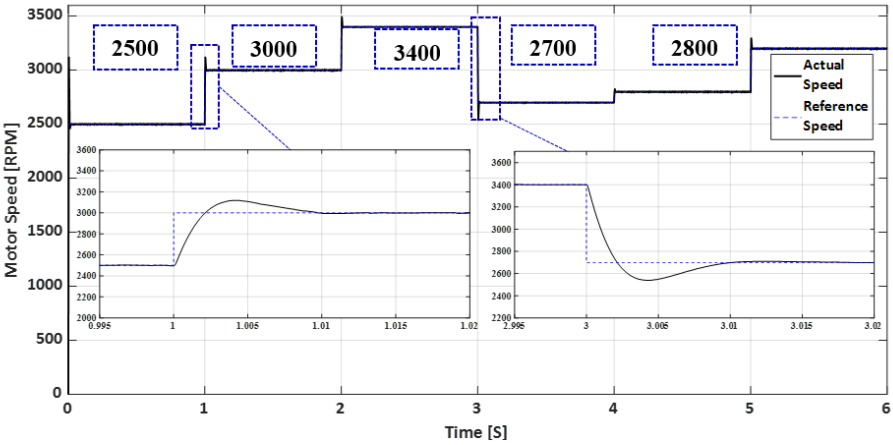

Fig. 20. Motor reference and actual speed.

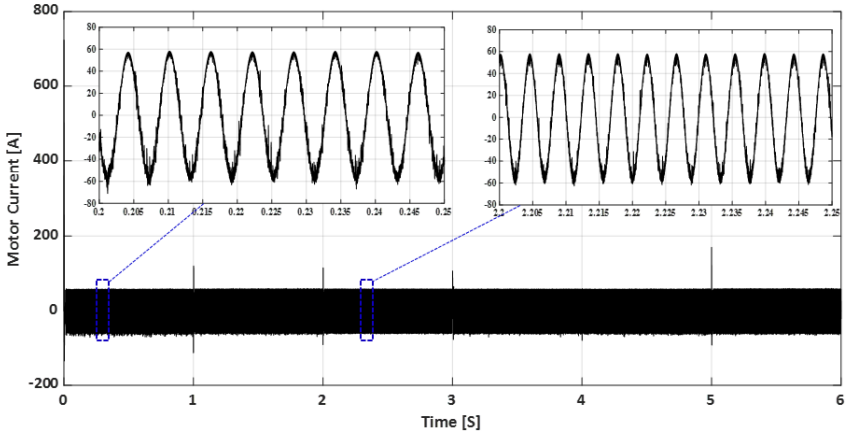

Fig. 21. Motor current (phase A).

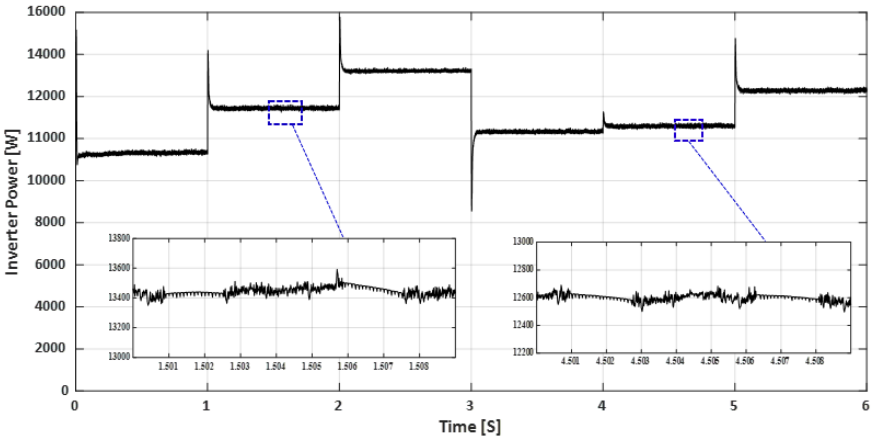

Fig. 22. Inverter (motor) avg. power.

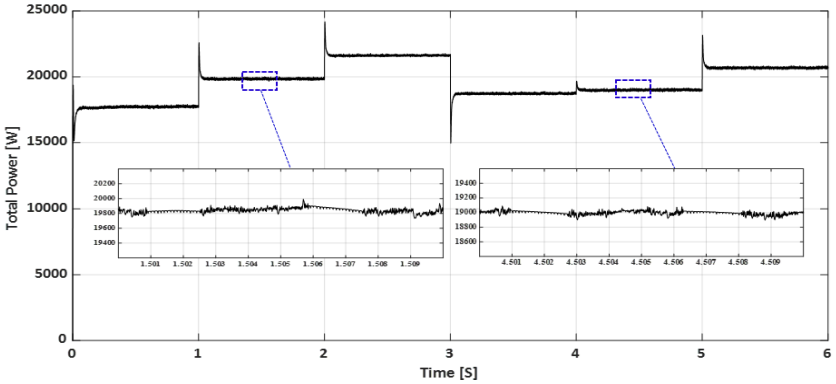

Fig. 23. Total system avg. power.

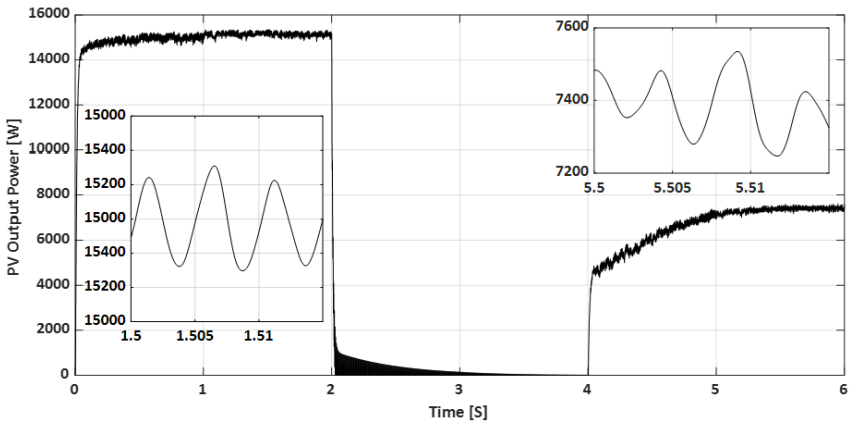

Fig. 24. PV output power under different irradiance values.

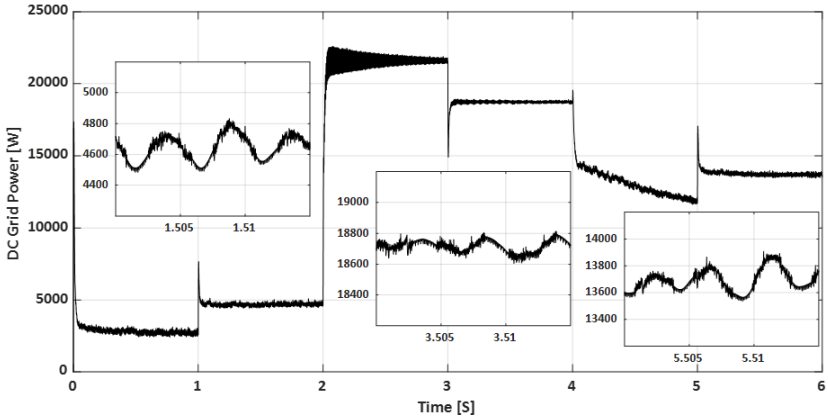

Fig. 25. DC grid avg. power.

Case study (2): The train moves under non-uniform irradiance conditions:

In order to accomplish PSC, Varying irradiance values are applied to each set of PV modules. This results in both local and global MPP, as demonstrated in Fig. 27. As a result, when P&O approach is used in this situation, Output power is trapped at a local MPP, as indicated in Fig. 26. It isn't valid here to operate with this low efficiency, therefore, PSO strategy is employed in this case to extract global MPP, with global voltage as indicated in Figs. (26-28). Fig. 32 displays reference speed and the motor speed simulation results. The same events mentioned in case study (1) are described in Table 5. As shown in Fig. 32 and Table 5, the change in speed using the FOC method works effectively during speed changes at a constant load, regardless of the light radiation received on the PV. Furthermore, it is characterized by its rapid response time; even under the worst conditions, it takes only 0.19 seconds to stabilize at the required speed with a dispersion level not exceeding 6%.

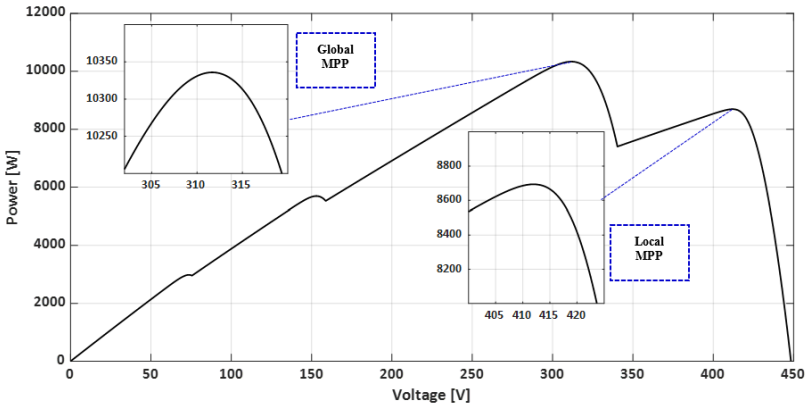

Fig. 26. Power vs voltage curve under PSC.

Fig. 31 shows the phase (A) motor current, it is studied at the same events mentioned in case study (1), which has a peak fundamental value of 55.87 A with THD = 3.21% as shown in Fig. 30 in the first indicated event and a peak fundamental value of 56.01 A with THD = 2.55% as shown in Fig. 31 in the second indicated event. Figs. (26, 34-36) display generated power from the PV system, shared power by the DC grid and consumed power in loads. Power analysis at different operating events is summarized in Table 6.

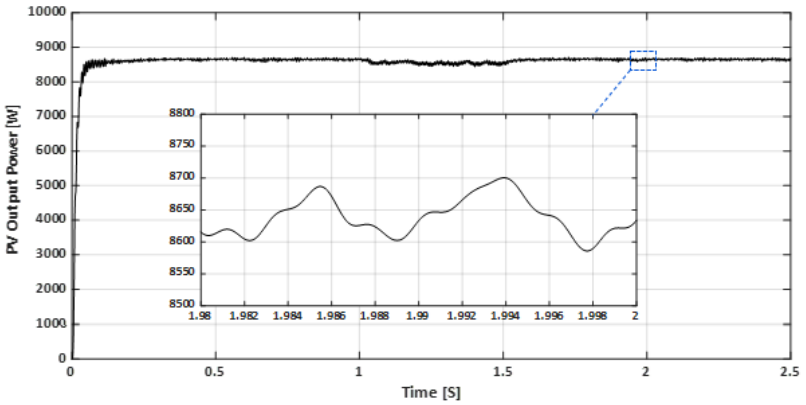

Fig. 27. PV output power by using P&O approach under PSC.

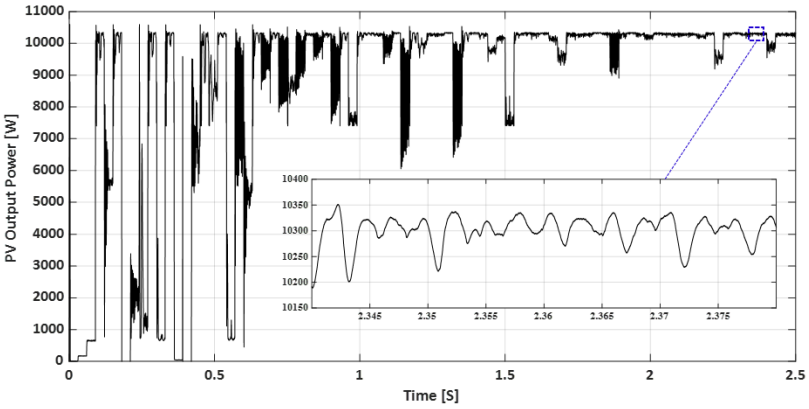

Fig. 28. PV output power under different irradiance values.

Table 5. Motor speed results analysis.

Steady state speed	3000	2700	RPM
Settling time	0.019	0.018	Sec
Peak transient speed	3117	2709.5	RPM
Min. transient speed	2993	2538.6	RPM
Overshoot	+3.9	-5.98	%

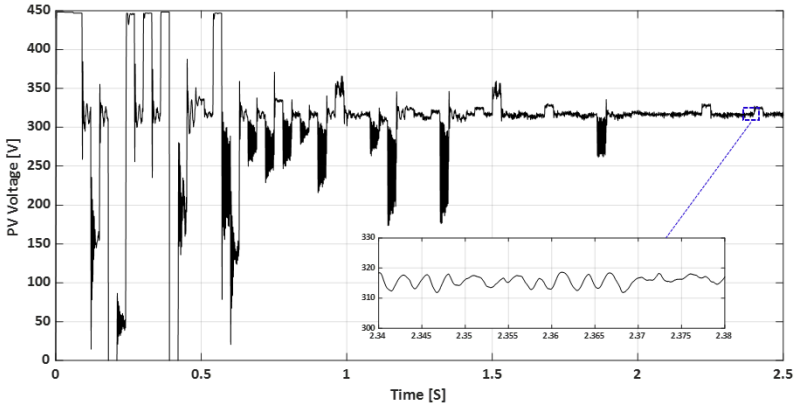

Fig. 29. PV voltage under different irradiance values.

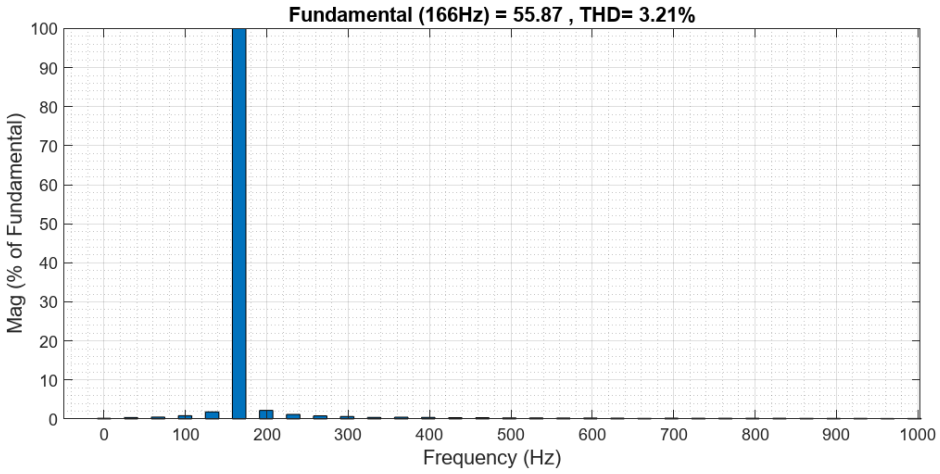

Fig. 30. THD of PMSM Current at 2500 RPM.

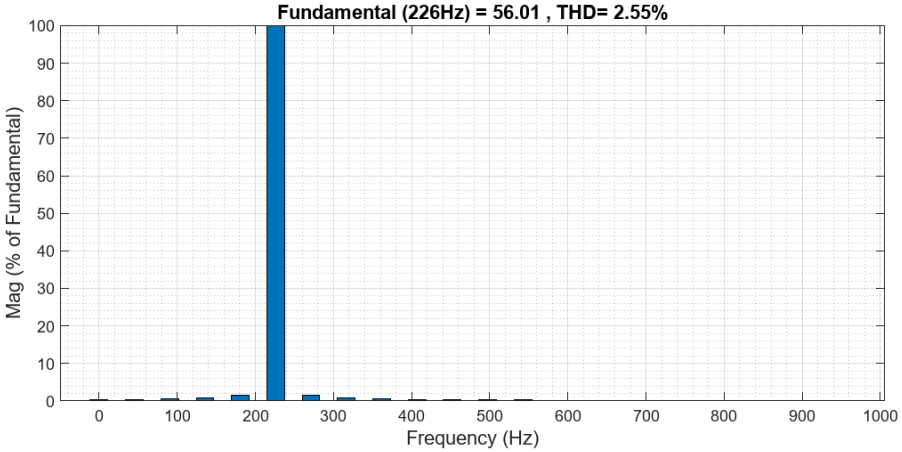

Fig. 31. THD of PMSM Current at 3400 RPM.

Table 6. System power analysis.

Conditions [25℃]	Motor speed [RPM]			2700			2800		
Loads [Kw]	Minimum Instantaneous Value	Inverter Power	Maximum Instantaneous Value	7.88	11.6	11.61	12.005	12.06	12.525
		DC Load Power		6.4			6.4		
		Total System Avg. Power		14.28	18	18.01	18.405	18.43	18.925
Sources [Kw]		PV Power		10.3					
		DC Grid Avg. Power		4.335	7.7	10.39	8.035	8.13	8.855

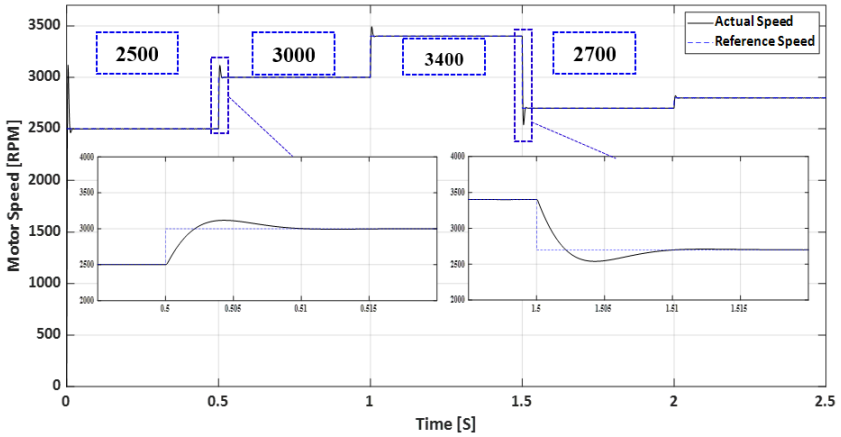

Fig. 32. Motor reference and actual speed.

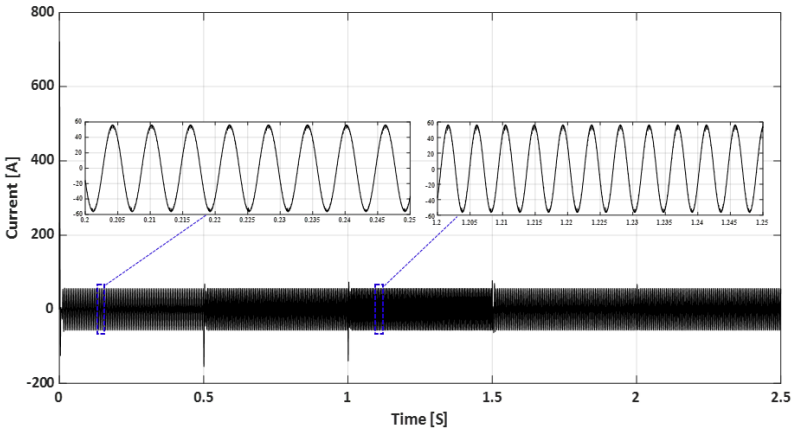

Fig. 33. Motor current (Phase A).

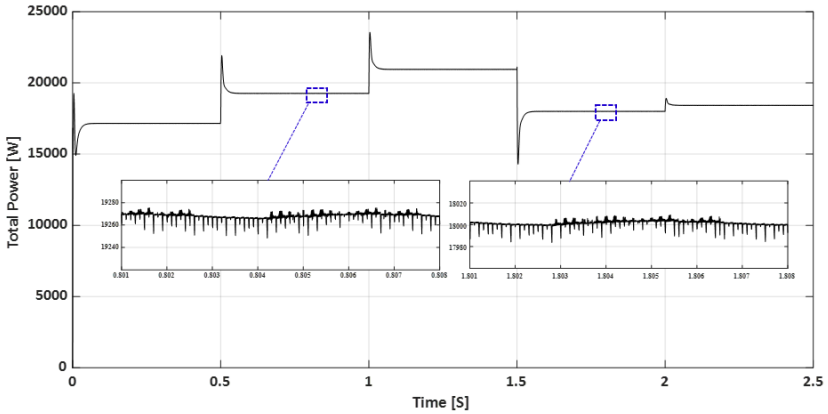

Fig. 34. Inverter (Motor) avg. power.

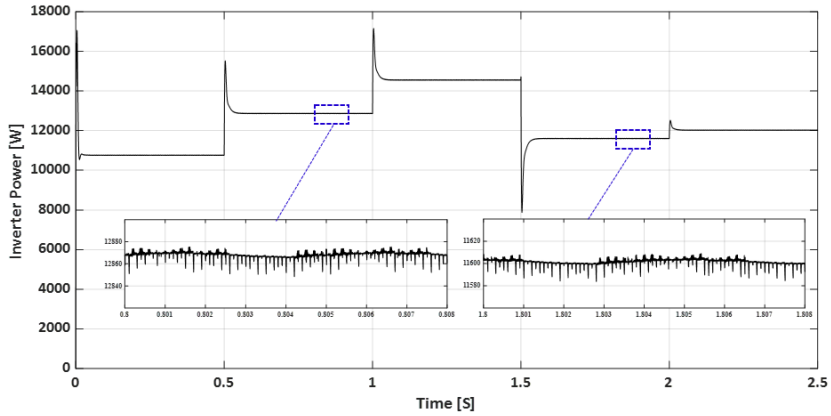

Fig. 35. Total system avg. power.

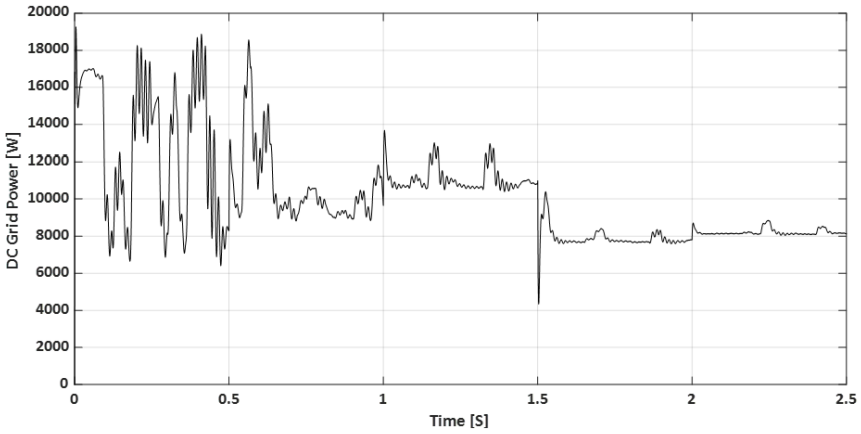

Fig. 36. DC grid avg. power.

Table 7. Comparison of different MPPT techniques [23].

Tracking Methods	Complexity	Cost	Response	Stability	Periodic Tuning	Suitable For Train Application
Suggested Technique	Medium	Affordable	Medium	Stable	Yes	Yes
Neural Network Technique	High	Expensive	Medium	Stable	No	No
Cuckoo Search Technique	Low	Very Expensive	Fast	Stable	No	No
Grey Wolf Optimization Technique	Medium	Affordable	Medium	Stable	Yes	Yes
Fuzzy Logic Controller Technique	High	Affordable	Medium	Stable	Yes	Yes

Based on the comparison, we consider the suggested approach is one of the promising ways to extract global MPP from an existing PV system in railway applications.

Financial Analysis and The Yearly Energy Production Calculations: Since the proposed system capacity is approximately 15.5 KW, taking into account a performance ratio of 0.8, which represents the losses caused by inverter, temperature, soiling, wiring, and mismatch losses. Based on solar atlas data average peak sun hours (PSH) along the train's route between the beginning and end of the trip is 6.2 h/day. With average Operation 345 days/year, considering that train maintenance takes around 20 days/year. The net energy extracted from the proposed system during the year equals 26,651.94 KWh/year. With a cost per kilowatt-hour of about 215 Egyptian piasters [38], the suggested system saves about 57,301.67 Egyptian pounds annually when operating a single train car.

Several vendors were interviewed to calculate the average cost of the suggested system. The average cost of the inverter was 250,000 Egyptian pounds, while the solar panels were 245,000 Egyptian pounds. in addition to the average cost of 100,000 Egyptian pounds for the metering device, protection system, mounting equipment, wiring, installation, and post-installation system testing. Consequently, the proposed system will cost an average of 595,000 Egyptian pounds. As a result, the suggested system's payback period was determined to be no more than 10.5 years. Taking into account the system's 25-year lifespan, this leaves around 14.5 years to make 837,741 Egyptian pounds savings from a single train car as indicated in Fig. 37. Additionally, an evaluation of the proposed system's environmental effect revealed lower CO_2 emissions. Since generating one kilowatt-hour from conventional sources produces approximately 997.6 grams of CO_2 [39], the proposed system would save approximately 26.5 tons of CO_2 annually when running a single train car.

Also, among the challenges and obstacles facing the proposed system, which are the main effects resulting from vibrations, can be summarized as follows: Microcracks, separation of layers, Mechanical failures in terms of installation and deviation from the specified mounting location, and deterioration of PV panel performance by up to 30%. One of the proposed solutions to address and avoid this problem is the use of specialized panels made of

thin or flexible photovoltaic cells, installed using flexible connectors and fasteners such as rubber to absorb vibrations caused by train movement.

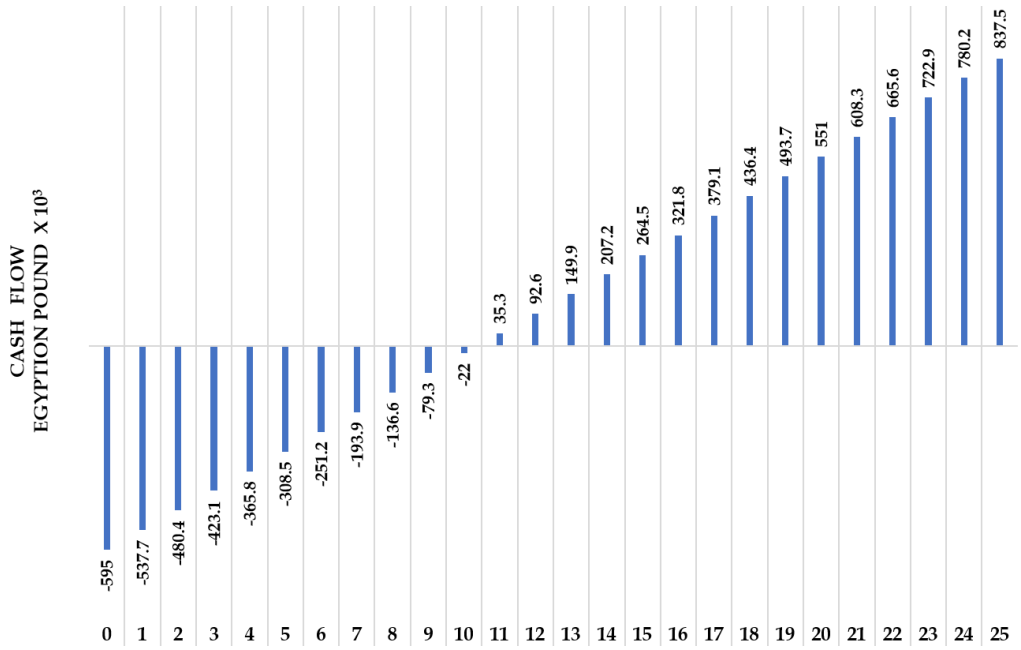

Fig. 37. Cash flow for the coming years.

6. CONCLUSIONS

This study focuses on installing photovoltaic systems directly on train roofs to contribute to system load supply. The system's performance was negatively impacted by the PSC problem. According to the simulation outcomes, the PMSM functioned well across a range of speed scenarios, and the P&O can effectively track MPP of PV modules in conditions of uniform irradiance. However, P&O is unable to follow the global MPP through PSC, which decreases the advantage of the PV system as it is trapped in a local MPP. For this reason, the control technique is switched to the PSO technique, which performs better than the P&O approach in tracking global MPP of and providing current with improved THD as indicated before, which gives a more efficient PMSM operation. The PSO strategy uses a live interaction with any irradiance variation. It operates to find the new global point and utilize power at this point to make the system more reliable and efficient.

According to the system financial Analysis. With a payback period of no more than 10.5 years which represent 42% of system lifetime and a total cost of 595,000 Egyptian pounds, the suggested system will also save 837,741 Egyptian pounds over the course of its lifespan which represent 1.40 times of the system cost. From an economic and financial standpoint, the system is appealing and promising because of all of this.

Additionally, reduced CO_2 emissions were found in an assessment of the proposed system's environmental impact. When operating a single train car, the suggested solution would save around 26 tons of CO_2 each year. Compared with other MPPT methods, the suggested approach is one of the successful ways to extract global MPP from an existing PV system in railway applications.

As a result, the project is appealing from a technical, financial, and environmental standpoint. It also offers a chance to fulfill regional and worldwide goals for sustainable growth and energy supply while protecting the environment.

For future work, the following is recommended:

The usage of modern MPPT techniques to investigate the electrical system performance on the trains. investigating the system's performance and economic viability when energy storage components like supercapacitors or upgraded batteries are present. examine the system's performance using a PV

module based on the two-and three-diode model, assess the performance, and contrast the outcomes with those from the one-diode PV model. examining the suggested system's actual implementation, detailing predicted challenges, and identifying suitable ways to get around them.

REFERENCES

[1] X. Dai, M. Chen, J. Lai, Y. Chen, T. Chen, N. Zhao, "Negative sequence compensation method for high-speed railway with integrated photovoltaic generation system," *CPSS Transactions on Power Electronics and Applications*, vol. 7, no. 2, pp. 130-138, 2022, doi: 10.24295/CPSSTPEA.2022.00012.

[2] K. Wang, H. Hu, J. Chen, J. Zhu, X. Zhong, Z. He, "System-level dynamic energy consumption evaluation for high-speed railway," *IEEE Transactions on Transportation Electrification*, vol. 5, no. 3, pp. 745-757, 2019, doi: 10.1109/TTE.2019.2934942.

[3] F. Ma, X. Wang, L. Deng, Z. Zhu, Q. Xu, N. Xie, "Multiport railway power conditioner and its management control strategy with renewable energy access," *IEEE Journal of Emerging and Selected Topics in Power Electronics*, vol. 8, no. 2, pp. 1405-1418, 2020, doi: 10.1109/JESTPE.2019.2899138.

[4] J. Kaleybar, H. Hafezi, H. Brenna, R. Faranda, "Smart AC-DC coupled hybrid railway microgrids integrated with renewable energy sources: current and next generation architectures," *Energies*, vol. 17, no. 5, p.1179, 2024, doi: 10.3390/en17051179.

[5] D. Fonseca-Soares, S. Eliziário, J. Galvincio, A. Ramos-Ridao, "Greenhouse gas emissions in railways: systematic review of research progress," *Buildings*, vol. 14, no. 2, 2024, doi: 10.3390/buildings14020539.

[6] International Energy Agency (IEA), *World Energy Outlook 2024*, Paris, France, 2024.

[7] P. Priya, A. Stonier, "Advancements in maximum power point tracking (MPPT) techniques for solar photovoltaic (PV) applications: a comprehensive review," *Energy Conversion and Management: X,* vol. 29, p. 101438, 2026, doi: 10.1016/j.ecmx.2025.101438.

[8] M. Elbelkasi, E. Badran, M. Abdel-Rahman, "Overview of DC and AC electric railway systems considering energy efficiency enhancement methods," *Port-Said Engineering Research Journal*, vol. 29, 2025, doi: 10.21608/pserj.2019.18206.1012.

[9] Z. Li, J. Pi, Y. Cao, Y. Wu, Z. Jia, "Research on transient low-frequency oscillation of electrified railway vehicle-grid coupling system," *IEEE Access*, vol. 11, pp. 29483-29499, 2023, doi: 10.1109/ACCESS.2023.3261126.

[10] M. Islam, A. Al Mamun, M. Ali, R. Ashique, A. Hasan, M. Hoque, M. Maruf, M. Al Mansur, A. Shihavuddin, "Integrating PV-based energy production utilizing the existing infrastructure of MRT-6 at Dhaka, Bangladesh," *Heliyon*, vol. 10, no. 2, 2024, doi: 10.1016/j.heliyon.2024.e24078.

[11] The World's First Solar-Powered Train in Australia, 2019, https://www.bridgestone.com/bwsc/stories/article/2019/06/17-2.html

[12] The Byron World First Solar Train, https://byronbaytrain.com.au/sustainability/.

[13] K. Abdulmawjood, W. Morsi, "Analyzing partial shading in PV Systems using wavelet packet transform and empirical mode decomposition techniques," *IEEE Access*, vol. 13, pp. 56085-56099, 2025, doi: 10.1109/ACCESS.2025.3552733.

[14] N. Haegel, S. Kurtz, "Global progress toward renewable electricity: tracking the role of solar," *IEEE Journal of Photovoltaics*, vol. 11, no. 6, pp. 1335-1342, 2021, doi: 10.1109/JPHOTOV.2021.3104149.

[15] IEA, *Global Energy Review 2025*, Paris, France, 2025.

[16] I. Jo, J. Lee, H. Lee, J. Lee, J. Lim, S. Kim, C. Park, "Analysis of optimal rotors skew to improve the total harmonic distortion of back electromotive force in MG-PMSM for traction," *IEEE Access*, vol. 11, pp. 122231-122237, 2023, doi: 10.1109/ACCESS.2023.3329113.

[17] P. Han, U. Seo, S. Paul, J. Chang, "Computationally efficient stator AC winding loss analysis model for traction motors used in high-speed railway electric multiple unit," *IEEE Access*, vol. 10, pp. 28725-28738, 2022, doi: 10.1109/ACCESS.2022.3158647.

[18] H. Tripathi, K. Marahatta, B. Gupta, N. Yadav, S. Shrestha, "Modelling and simulation of field-oriented control of permanent magnet synchronous motor," *Journal of Engineering and Sciences,* vol. 2, no. 1, 2023, doi: 10.3126/jes2.v2i1.60412.

[19] S. Paul, P. Han, J. Chang, Y. Chun, J. Lee, "State-of-the-art review of railway traction motors for distributed traction considering South Korean high-speed railway," *Energy Reports*, vol. 8, pp.14623-14642, 2022, doi: 10.1016/j.egyr.2022.10.411.

[20] X. Geng, B. Zhang, D. Qiu, Y. Chen, W. Xiao, F. Xie, "Modeling and nonlinear dynamic analysis of a photovoltaic system with multiple parallel branches based on simplified discrete time model," *IEEE Transactions on Power Electronics*, vol. 39, no. 8, pp. 10226-10238, 2024, doi: 10.1109/TPEL.2024.3388577.

[21] E. Özkalay, F. Valoti, M. Caccivio, A. Virtuani, G. Friesen, C. Ballif, "The effect of partial shading on the reliability of photovoltaic modules in the built-environment," *EPJ Photovolt Special Issue on 'EU PVSEC 2023*, vol. 15, no. 7, p. 17, 2024, doi: 10.1051/epjpv/2024001.

[22] T. Nagadurga, V. Raju, A. Barnawi, "Global MPPT optimization for partially shaded photovoltaic systems," *Science Reports,* vol. 15, p. 10831, 2025, doi: 10.1038/s41598-025-89694-7.

[23] M. Katche, A. Makokha, S. Zachary, M. Adaramola, "A comprehensive review of maximum power point tracking (MPPT) techniques used in solar PV systems," *Energies*, vol. 16, no. 5, p. 2206, 2023, doi: 10.3390/en16052206.

[24] H. Abidi, L. Sidhom, I. Chihi, "Systematic literature review and benchmarking for photovoltaic MPPT techniques," *Energies*, vol. 16, no. 8, p. 3509, 2023, doi: 10.3390/en16083509.

[25] K. Abdulmawjood, S. Alsadi, S. Refaat, W. Morsi, "Characteristic study of solar photovoltaic array under different partial shading conditions," *IEEE Access*, vol. 10, pp. 6856-6866, 2022, doi: 10.1109/ACCESS.2022.3142168.

[26] H. Ahessab, A. Gaga, B. Elhadadi, "Enhanced MPPT controller for partially shaded PV systems using a modified PSO algorithm and intelligent artificial neural network, with DSP F28379D implementation," *Science Progress,* vol. 107, no.4, 2024, doi: 10.1177/00368504241290377.

[27] "The National Agenda for Sustainable Development Egypt's Updated Vision 2030," *Ministry of Planning and Economic Development*, 2023.

[28] Global Solar Atlas Website, https://globalsolaratlas.info/map?c=11.523088,8.173828,3.

[29] G. Abad, *Power Electronics and Electric Drives for Traction Applications*, Hoboken, NJ, USA: Wiley, 2017

[30] S. Paul, J. Lee, P. Han, J. Chang, Y. Chun, V. Khanh, "Bi-directional coupled electro-thermal behaviors of traction motor for high-speed railway distributed traction system," *Case Studies in Thermal Engineering,* vol. 49, p. 103248, 2023, doi: 10.1016/j.csite.2023.103248.

[31] A. Podder, N. Roy, H. Pota, "MPPT methods for solar PV systems: a critical review based on tracking nature," *IET Renewable Power Generation*, vol. 13, no. 10, pp.1615-1632, 2019, doi: 10.1049/iet-rpg.2018.5946.

[32] T. Hashemi, R. Mahboobi, H. Jafari, "Composite switched lyapunov function-based control of DC–DC converters for renewable energy applications," *Electronics*, vol. 13, no. 1, 2024, doi: 10.3390/electronics13010084.

[33] P. Chavan, D. Gowda, S. Nayak, "Field oriented control technique for PMSM," International Conference ICAMIDA, 2023, doi: 10.2991/978-94-6463-136-4_41.

[34] S. Sakunthala, R. Kiranmayi, P. Mandadi, "A study on industrial motor drives: Comparison and applications of PMSM and BLDC motor drives," International Conference ICECDS, 2017, doi: 10.1109/ICECDS.2017.8390224.

[35] X. Li, D. Xi, Y. Zhang, "Permanent magnet synchronous motor vector control based on MATLAB/Simulink," First International Conference on Electronics Instrumentation & Information Systems, 2017, doi: 10.1109/EIIS.2017.8298737.

[36] A. Baba, G. Liu, X. Chen, "Classification and evaluation review of maximum power point tracking methods," *Sustainable Futures*, vol. 2, p. 100020, 2020, doi: 10.1016/j.sftr.2020.100020.

[37] X. Tang, Z. Zhang, X. Liu, C. Liu, M. Jiang, Y. Song, "A Novel field-oriented control algorithm for permanent magnet synchronous motors in 60° coordinate systems," *Actuators*, vol. 12, no. 2, p. 92, 2023, doi: 10.3390/act12020092.

[38] Daily Economic Update, "*Economic Reports, National Bank of Kuwait – Egypt,*" 2024.

[39] Q. Zhang, K. Qiao, C. Hu, P. Su, O. Cheng, N. Yan, L. Yan, "Study on life-cycle carbon emission factors of electricity in China," *International Journal of Low-Carbon Technologies,* vol. 19, pp. 2287–2298, 2024, doi: 10.1093/ijlct/ctae181.